

## ACTIVE MATTER

# Collective clog control: Optimizing traffic flow in confined biological and robophysical excavation

J. Aguilar<sup>1\*</sup>, D. Monaenkova<sup>2\*</sup>, V. Linevich<sup>1</sup>, W. Savoie<sup>2</sup>, B. Dutta<sup>3</sup>, H.-S. Kuan<sup>4</sup>, M. D. Betterton<sup>5</sup>, M. A. D. Goodisman<sup>6</sup>, D. I. Goldman<sup>2†</sup>

Groups of interacting active particles, insects, or humans can form clusters that hinder the goals of the collective; therefore, development of robust strategies for control of such clogs is essential, particularly in confined environments. Our biological and robophysical excavation experiments, supported by computational and theoretical models, reveal that digging performance can be robustly optimized within the constraints of narrow tunnels by individual idleness and retreating. Tools from the study of dense particulate ensembles elucidate how idleness reduces the frequency of flow-stopping clogs and how selective retreating reduces cluster dissolution time for the rare clusters that still occur. Our results point to strategies by which dense active matter and swarms can become task capable without sophisticated sensing, planning, and global control of the collective.

Diverse living (1) and artificial (2) active materials (3) and swarms spontaneously form clusters that can persist for long durations. However, for tasks that demand steady flow, such formations can be disadvantageous: Confined active systems such as pedestrian or vehicular traffic jams (4), competing bacterial biofilms (5), high-density migrating cells (6), jammed herds (7), and robot swarms (8) can produce high-density clogs that readily form glasslike arrests of flow (9). In such systems, the ability to dissolve clusters and prevent their formation (9), particularly in the absence of global knowledge of the state of all elements, is crucial.

Social insects (10) perform many tasks that demand clog minimization and mitigation. Substrate excavation specialists such as fire ants (*Solenopsis invicta*) cooperatively create nests of complex subterranean networks (Fig. 1A) consisting of tunnels in soil that support bidirectional traffic without lanes (11). Our previous laboratory experiments (12) revealed that, in the early stages of nest construction, the few-millimeter-long ants construct vertical tunnels approximately one body length in diameter (13). These narrow tunnels benefit the climbing ants as they transport bulky pellets, because close proximity to walls allows limbs, body parts, and antennae to aid slip recovery (12). But although

the structure of the tunnels seems to benefit individuals, physical-model experiments make it clear that excavation can suffer as a result of clogging during high-traffic conditions [e.g., (14) and Fig. 1C]. Here we use biological, theoretical, computational, and robophysical systems to show that counterintuitive behaviors—individual idleness and retreating—help optimize tunnel density by limiting the severity and prevalence of clogs, thereby enabling rapid excavation by the collective.

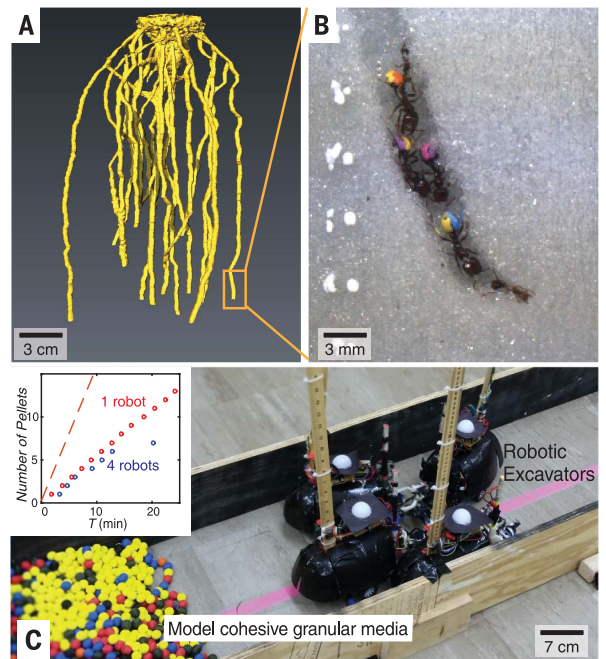
In laboratory experiments, we monitored the activity of fire ants as they excavated a cohesive

granular medium. Groups of ~30 workers were placed in transparent containers containing particle-water mixtures (13) consisting of 0.25-mm-diameter glass particles (Fig. 2A) with a soil moisture content, defined as the ratio of total water weight to total solid weight, of 0.01 or 0.1 (three trials each) (13). Ants excavated for 48 hours, with individual ants entering and exiting the tunnel hundreds of times. As in our previous study (12), ants constructed narrow vertical tunnels by means of a stereotyped process of grain and multigrain (pellet) removal and transport, followed by tunnel ascent and substrate deposition upon exit (13). A camera mounted to a motorized linear stage tracked a region within about three body lengths from the tunnel face (Fig. 2A and supplementary materials). We distinguished individual ant activity by marking ant abdomens with different colors (Fig. 1B). We recorded tunnel length over time (Fig. 2B), and the presence of each worker was logged when in the camera's view (Fig. 2C).

Ants exhibited a variety of behavioral tasks during collective excavation. A large fraction ( $0.22 \pm 0.1$  for soil moisture content of 0.01 and  $0.31 \pm 0.13$  for soil moisture content of 0.1) of ants never entered the tunnel to excavate during the 48-hour period of observation; we refer to these as “nonvisitors.” As seen in Fig. 2C, ants that visited the tunnel face (“visiting” ants) varied in activity level. Inspired by work in honey bees (15), we quantified activity inequality among visitor ants using Lorenz curves. Points on the Lorenz curves in Fig. 2D link the cumulative fraction of workers in the population to the cumulative share of activity by that fraction. Although visitor ants' trips did not always result in the extraction of a pellet (see movie S1 and discussion

## Fig. 1. Confined and crowded biological and robotic excavators.

(A) X-ray reconstruction of *S. invicta* fire ant excavation in a large container (25 cm wide) filled with 240- to 270- $\mu$ m-diameter glass particles (supplementary materials). (B) Painted *S. invicta* workers excavating a single tunnel along the wall of a transparent container with 0.25-mm-diameter wet glass particles. (C) Autonomous robotic diggers excavating in a simulated environment with cohesive granular media (diameter of 1.8 cm). The inset shows the number of pellets (defined as a cohesive group of grains) deposited versus time (7) by a robot excavating alone (red dots) and the net excavation of four robots (blue circles), whereby each robot attempts to excavate maximally. Orange dashed line indicates the hypothetical performance of the group of four robots in the absence of confinement.



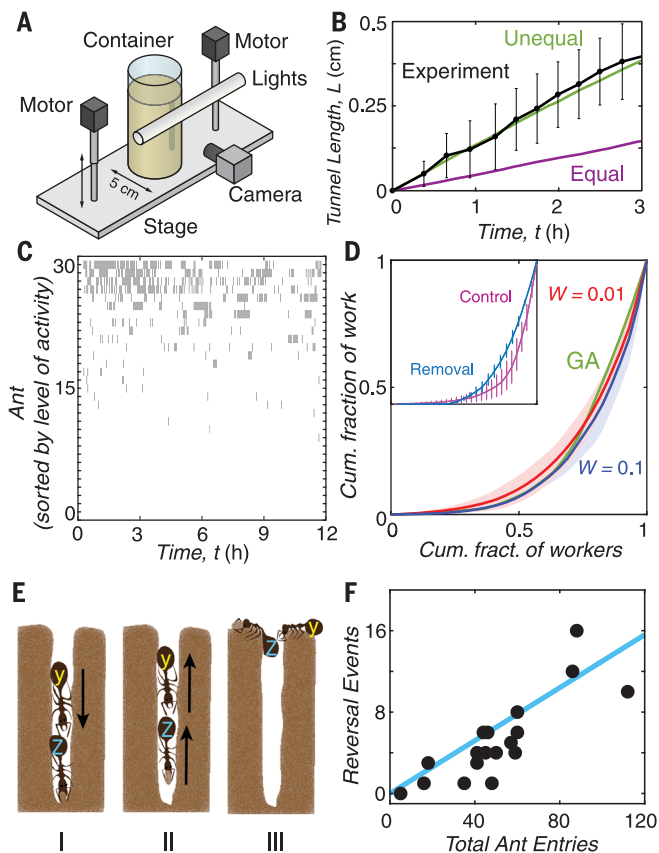
<sup>1</sup>School of Mechanical Engineering, Georgia Institute of Technology, Atlanta, GA 30332, USA. <sup>2</sup>School of Physics, Georgia Institute of Technology, Atlanta, GA 30332, USA.

<sup>3</sup>School of Electrical and Computer Engineering, Georgia Institute of Technology, Atlanta, GA 30332, USA. <sup>4</sup>Max Planck Institute for the Physics of Complex Systems, Nöthnitzer Str. 38, 01187 Dresden, Germany. <sup>5</sup>Department of Physics, University of Colorado Boulder, Boulder, CO 80309, USA. <sup>6</sup>School of Biological Sciences, Georgia Institute of Technology, Atlanta, GA 30332, USA.

\*These authors contributed equally to this work.  
†Corresponding author. Email: daniel.goldman@physics.gatech.edu

## Fig. 2. Biological observations reveal workload inequality and reversal behaviors in ants.

(A) Experimental apparatus to track ant excavation; the inner diameter of the container is 5.21 cm. (B) The growth of tunnel length over time. Shown are average experimental results  $\pm$  SD/2 for *S. invicta* workers (black) and simulations for groups with equal (purple) and unequal (green) workload distribution. Error bars denote 1 SD in each direction. (C) “Visitation” map derived from experimental data. Each point in the map indicates the presence of a particular ant (out of 30 ants), ordered from most active (y axis) in the tunnel at a time  $t$  [soil moisture content ( $W$ ) of 0.1]. (D) Lorenz curves for workload distributions obtained in wet



0.25-mm-diameter glass particles with soil moisture content of 0.1 (blue) and 0.01 (red) and a CA model (green) whose excavation rate was optimized with a GA. Shaded areas correspond to standard deviation from three experiments. cum., cumulative. The inset shows average Lorenz curves  $\pm$  SD/2 for a workload distribution within the group before (control, purple) and after (removal, blue) the most active diggers are removed from the group. Error bars correspond to standard deviations from three experiments. (E) Illustration of observed reversal behavior. (I) Ant Y's path to excavate is blocked by ant Z. (II) After Z collects a pellet, it reverses, (III) forcing Y to reverse without excavating. (F) Total number of reversal events versus total ant visitors for the first 3 hours of ant excavation (soil moisture content of 0.1). Each data point represents total reversal events and total entries counted for 30-min segments collected from three experiments. Linear fit (blue line) with coefficient of determination ( $R^2$ ) = 0.69.

below), we included these “reversals” in the Lorenz curve calculations because these animals expended energy in a trip to the tunnel face and contributed to tunnel traffic.

To characterize the Lorenz distributions, we calculated the Gini coefficient,  $G$ , defined as the ratio of the area between the Lorenz curve and the line of equality to the area under the line of equality (15).  $G$  is a measure of the deviation of the workload from perfectly shared ( $G = 0$ , all workers work equally) to completely unshared ( $G = 1$ , a single worker performs all work). Lorenz curves were characterized by  $G = 0.75 \pm 0.10$  and displayed similar functional forms across a variety of experimental conditions (see Fig. 2D and fig. S2).

In the presence of competing tasks, like foraging or brood care, task allocation in ants can change depending on colony needs (16). To investigate temporal variation in ant excavation workload, we divided 48-hour experiments into

12-hour “epochs” (time periods). Although individual activity varied among epochs (Fig. 2C and fig. S3), the cumulative workload distribution was independent of epoch [one-way analysis of variance (ANOVA)  $F_{3,20} = 0.85$ ,  $P = 0.48$ ] and soil moisture content (one-way ANOVA,  $F_{1,23} = 2.54$ ,  $P = 0.13$ ) (Fig. 2D, figs. S1 and S2, and table S1). Furthermore, when the most active excavators were removed from the group, remaining workers increased their activity and compensated for the loss, preserving the shape of the Lorenz curve and therefore producing similar Gini coefficients (one-way ANOVA,  $F_{1,4} = 1.13$ ,  $P = 0.35$ ) (Fig. 2D, inset; table S2; and supplementary materials). Thus, given the consistency of the workload distribution, we hypothesize that variations in idleness (low activity levels) within a population may play an adaptive role in modulating the crowded conditions of confined tunnels and could have been important in the earliest social insect colonies (17).

Reversal behaviors were characterized by ants entering the tunnel and returning to the exit without carrying soil pellets. During the first 3 hours of the experiments, reversals occurred for  $26 \pm 13\%$  of trips for soil moisture content of 0.01 and  $18 \pm 3\%$  of trips for soil moisture content of 0.1. These events were often associated with local crowding at the excavation face (Fig. 2E) ( $16 \pm 12\%$  of trips for soil moisture content of 0.01 and  $10 \pm 2\%$  of observations for soil moisture content of 0.1). Reversal behaviors in crowded conditions occur on foraging trails (18), and similar phenomena have been observed in swarming bacteria (5). The incidence of this seemingly unproductive behavior increased with increasing overall activity of ants (Fig. 2F), suggesting that this behavior serves as a feedback mechanism for mitigating clogs during excavation.

To systematically examine the effects of idleness and individual retreating behaviors on excavation performance, we developed a cellular automata (CA) excavation model (Fig. 3A and supplementary materials). Such models are useful in elucidating the dynamics of biological and vehicular traffic (9, 19). The model consists of a lattice (the “tunnel”) with a width of two cells [similar to *S. invicta* tunnel widths (20)] occupied by soil, empty space, an ascending CA “ant,” and/or a descending CA ant (Fig. 3A). The CA ants can move, change directions, excavate, deposit a pellet, or rest. As in the biological experiments, activity for the workload distribution in the CA model was measured by counting instances when CA ants visited the tunnel within three body lengths (cells) of the excavation site.

We simulated the behavior of CA ants using both equal workload distributions (which we refer to as “active” CA ants) and unequal workload distributions (which we refer to as “Lorenz” CA ants) with identical reversal probabilities (movie S2). In unequal workload distributions, individual CA ants were assigned individual “entrance probabilities” defined as the probability that a CA ant will enter the tunnel. The initial entrance probability distribution for the 30 CA ants was taken from the biological distribution. Output workload distributions of CA simulations closely matched the input entrance probability distributions (as measured by the Gini coefficient, fig. S25). During a time-step, if its path toward the excavation area was blocked, a CA ant would reverse direction toward the exit with a probability,  $R$ , of 0.34 (supplementary materials);  $R$  was set by the proportion of total reversal events observed for 0.01 soil moisture in the biological experiments.

The CA model that used unequal workload distribution and reversals reproduced experimentally observed biological ant digging rates (Fig. 2B). To determine if these rates represented an optimal workload distribution, we used a genetic algorithm (GA) (fig. S24) to select for entrance probability distributions (supplementary materials) that maximized excavated tunnel length within a given duration. Regardless of the initial population distribution (either similar to the ants or highly unequal), within a

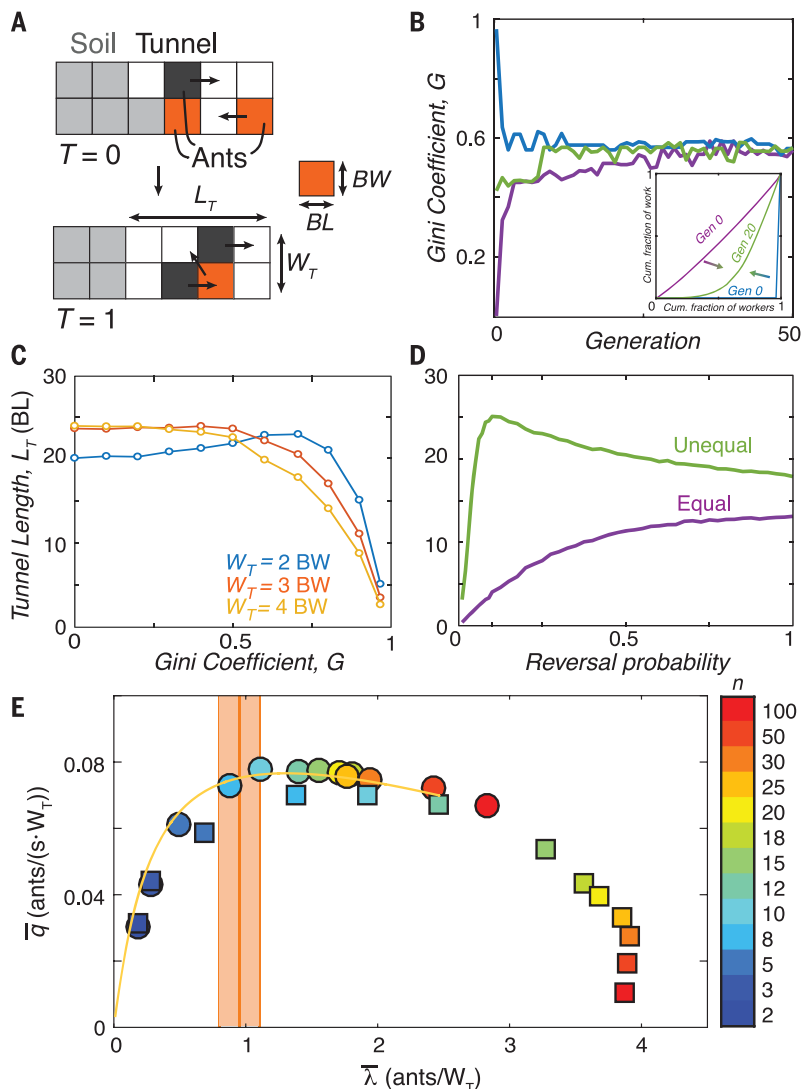


**Fig. 3. Models reveal optimized traffic flow in narrow tunnels by means of selective retreating and workload inequality.** (A) Schematic showing the main components of the CA model. Cell colors denote soil (light gray), tunnel (white), ants moving toward the excavation site (orange), and ants exiting the tunnel (dark gray).  $T$ , simulation time-step. (B) Gini coefficient over time under GA optimization for groups started with a completely equal (purple), completely unequal (blue), and random (green) workload distribution. Lorenz curves (inset) for groups that begin with complete equality or inequality rapidly reach a similar workload distribution. (C) Excavated tunnel length,  $L_T$ , after 24-hour simulation time versus Gini coefficient for tunnels of different widths,  $W_T$ , for a 30-CA ant population. BL, body length; BW, body width. (D) Excavated tunnel length after 24-hour simulation time versus reversal probability for equal and unequal (optimized for 30 CA ants) workload distributions. (E) Simulated traffic flow ( $\bar{q}$ , number of ants divided by time in seconds times tunnel width) versus CA ant occupancy ( $\bar{\lambda}$ , number of ants divided by tunnel width, measured in excavator body widths) for groups of equally (squares) and unequally (circles) active ants. Color bar indicates the size,  $n$ , of the excavating group. The theoretical fundamental diagram of the OAT model (yellow curve) illustrates the need to limit tunnel traffic to one worker per body width of tunnel width to optimize flow and prevent deleterious clogs. Experimental ant observations reveal an average occurrence around this density (orange-shaded region, where the orange centerline is the mean and the extents are one standard deviation away from the mean).

few generations, the GA simulation converged to an unequal workload distribution (Fig. 3B, for a 30-ant example), which was similar to the experimentally observed biological workload distributions (Fig. 2D, green).

The CA model also revealed the importance of the reversal behavior in conjunction with unequal workload distributions. Although the active excavation could be improved by sufficient reversal probability, only a small amount of reversal was

needed to increase the excavation performance in the unequal distribution (Fig. 3D). Thus, in addition to the benefits narrow tunnels provide for climbing and pellet transport (12, 13), we hypothesize that the ants benefit from narrow tunnels by expending less energy to dig wider tunnels to the same depth. Such benefits would be useful in the early stages of new nest construction (e.g., after the colony is flooded out) during which establishing the colony underground is critical.

To gain insight into other benefits and constraints set by such narrow tunnels, we simulated 30 CA ants with varied workload distributions (characterized by distinct Gini coefficients) in tunnels of different widths. These distributions were created through a randomized Monte Carlo process, such that the Lorenz curves resulted in desired Gini coefficients. A peak in excavated length,  $L$ , versus Gini coefficient was observed in a tunnel two cells wide (Fig. 3C). Wider tunnels (three and four cells wide) resulted in broader performance peaks, indicating a decreased sensitivity in performance owing to workload distribution. This indicates that use of a narrow tunnel necessitates the “discovery” of the unequal workload distribution of ants.

We hypothesized that the unequal workload distribution and reversals were linked to uniform flow of CA ants in the tunnel. We therefore measured the average flow rate of successful excavators,  $\bar{q}$ , versus the average tunnel-width-normalized occupancy of excavators,  $\bar{\lambda}$  (the ratio of average number of ants in the tunnel to tunnel width measured in ant body widths). To generate a wide range of average occupancies, we varied the population size of the CA system.

The flow rate was optimal at an intermediate occupancy (Fig. 3E). This nonmonotonic trend in  $\bar{q}$  versus  $\bar{\lambda}$  is characteristic of various multi-agent systems, including bridge-building army ants (21) and vehicle traffic (22, 23), and is referred to in traffic literature as the “fundamental diagram” (24). Active ants, which do not modulate their workload distribution, increase tunnel occupancy with increasing population and thus exhibit optimal flow rates for only a few population sizes. By contrast, GA-optimized Lorenz ants produced tunnel occupancies in the ideal range by generating increasingly unequal workload distributions for increasing CA ant population sizes. Of particular importance, fire ants produced tunnel densities in the ideal range (Fig. 3E, orange-shaded region).

The ability of the ants to operate at the optimum in the fundamental diagram and the rapidity by which the GA model converges (Fig. 3B) indicate the existence of a simple governing principle for traffic control in confined task-oriented systems. To elucidate this principle, we formulated a minimal model of ant traffic in the narrowest (single-lane) tunnel: the one-at-a-time (OAT) model. This model, which builds on recent work on traffic of motor proteins on microtubules (25), allows us to estimate analytically how the excavation rate varies with the rate of ants entering the tunnel (supplementary materials) for various work-distribution strategies.

In the OAT model, ants enter the tunnel and move toward its face; descending ants reverse direction if they either reach the end of the tunnel or collide with an ant moving in the other direction (supplementary materials). We initially modulated occupancy by varying the entrance probability of all ants equally; as in the CA model, the flow rate of the OAT model was optimal at an intermediate width-normalized ant occupancy (Fig. 3E, yellow curve, and supplementary materials)—in particular, one excavator for every excavator that can fit along the width of the tunnel. Although the peak in the fundamental diagram has been associated with the transition between steady flow and propagating traffic jams (24), the OAT model highlights a key feature of confined tunnel excavation: Traffic dynamics are driven by tunnel width. Given the task-oriented nature of the system, successful traffic flow is only possible if a worker can travel the entire length of the tunnel and back. Thus, if there are enough workers in the tunnel to clog the path to or from the excavation site, traffic is likely to slow down. The OAT model highlights this scenario, as such clogs are unavoidable if more than one ant is in the single-lane tunnel. Because ants cannot pass each other or change lanes, only the first ant to enter can reach the end to excavate, whereas other workers collide with the first worker, reverse, and impede traffic.

Mechanisms that target a specific number of excavators occupying the tunnel given the tunnel's width promote ideal traffic flow. When individual ants in the OAT model were programmed to modulate their rate of reentry according to how often they reversed without excavating, the OAT model rapidly converged to Lorenz curves similar to the biological and GA-optimized CA ants (supplementary materials and fig. S23). Such rapid convergence highlights the benefit of targeting a specific number of ants (in this case, by establishing unequal workload distributions) in narrow tunnels.

We next used a system of excavating robots (fig. S9) to test if the above theoretical strategies could improve traffic in confined experimental situations with more complex, unpredictable interactions. Because, presently, robot mobility in real-world environments is poor relative to biological systems and because real collisional interactions not modeled in CA and OAT are typically neglected in swarming robot studies (2), such robophysical (26) studies can aid robot design and control for real-world robot swarms, as well as suggest hypotheses for studies of ant traffic (18), adaptive behaviors, and morphological features for crowded excavation and movement.

Groups of roughly elliptical robots (movie S3) with similar aspect ratios to the biological ants were tasked with excavating a model cohesive granular medium of hollow plastic spheres containing loose magnets; this design allows clumps of media to be formed, analogous to the pellets of cohesive soil formed by the biological ants (13). Our robots followed simple instructions

triggered by onboard sensory feedback of the surrounding environment (supplementary materials). Previous work in swarm robotics (27) used similar decentralized strategies in conjunction with collision-avoidance schemes (2, 28) to produce emergent flocking behavior. By con-

trast, our robots detected collisions with push switches on their outer shell, which triggered navigation strategies such as steering away and readjusting to promote clog resolution (movie S4).

To challenge the robots, we constructed a tunnel (Fig. 4A) with a width of three robot

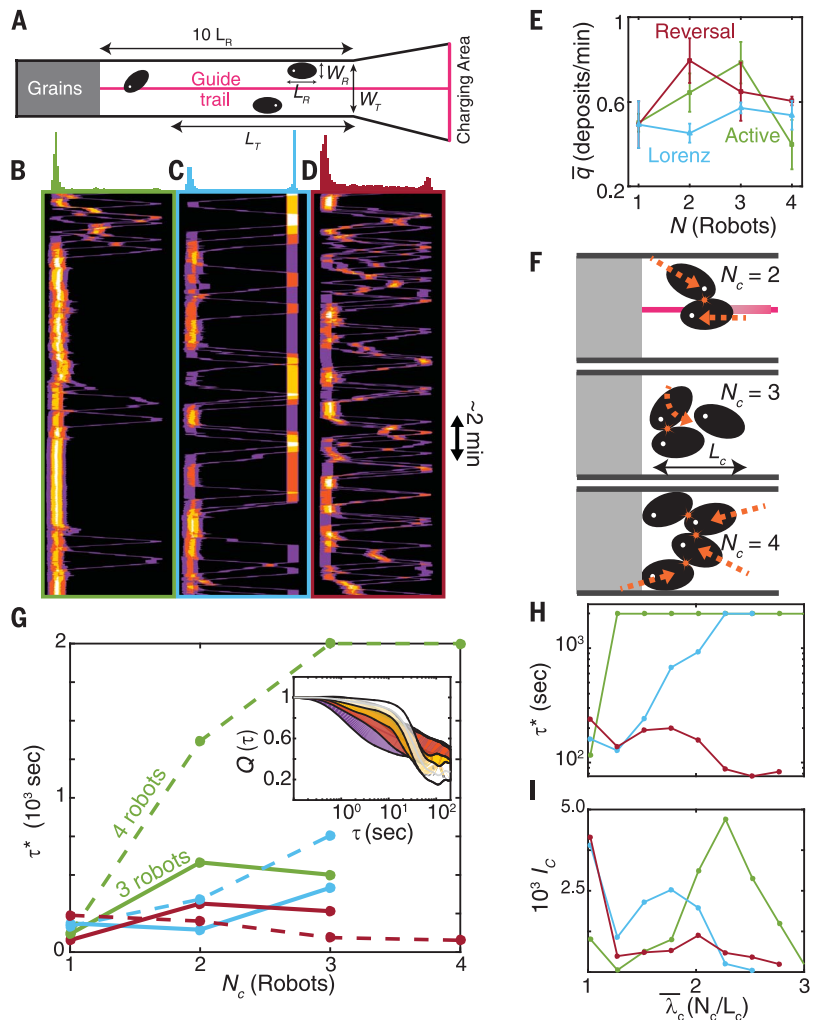


**Fig. 4. Traffic flow and local dynamics during robot excavation.** (A) Schematic of the excavation arena indicating the tunnel length,  $L_T$  (excluding the excavation area); robot width,  $W_R$ ; robot length,  $L_R$ ; and tunnel width,  $W_T$ . A pink centerline along the tunnel was monitored by the robots' onboard cameras, enabling them to follow the tunnel path. (B to D) Experimental space-time overlap heat maps of robot positions (x axis) for four-robot trials of (B) active digging, (C) Lorenz digging, and (D) reversal digging. Color indicates the number of robots occupying a particular space and time: one (purple), two (orange), three (yellow), and four (white) robots. Histograms above the graphs show the frequency of occurrence of clusters with two or more robots at different lateral positions. (E) Average flow rate,  $\bar{q}$ ,  $\pm$  SD measured in deposits per minute versus number of robots in the experiment,  $N$ , for active (green), Lorenz (light blue), and reversal (maroon) strategies. (F) Illustration of various collision scenarios encountered by robots owing to movement toward guide trail (top), turning (middle), and forward-backward translation (bottom). Orange starbursts indicate collisions. (G to I) Relaxation times for all strategies: active (green), Lorenz (light blue), and reversal (maroon). (G) Relaxation time versus cluster size,  $N_c$ , for three-robot (solid) and four-robot (dashed) trials. The inset shows sample average correlation curves,  $Q(\tau)$ , that measure how  $N_c = 1$  (purple), 2 (orange), 3 (yellow), and 4 (white) robot clusters dissolve over time during four-robot reversal trials; shaded region indicates average curves  $\pm$  SD/2 (standard deviations for  $\tau^*$  range from 100 to 500 s). (H) Relaxation times versus linear aggregation density,  $\bar{\lambda}_c$ , for four-robot trials and (I) corresponding number of cluster occurrences,  $I_c$ , versus linear aggregation density.

widths (or 1.5 robot lengths), which, combined with the oblong robot shape, forced a challenge of turning around in confined spaces. We tracked the positions (supplementary materials and fig. S10) of the robots in the main tunnel area (i.e., excluding the excavation site) to generate space-time overlap maps of robot positions (see Fig. 4, B to D), which give visual insight into robot flow during excavation.

We first examined systematically how excavation performance changed as numbers of robots increased for our active protocol (as in Fig. 1C and fig. S6), which assigned equal work “desire” to all diggers: After soil deposition, each robot immediately returned to the tunnel to excavate. Despite constraints on maneuverability, sensing, and morphology, the robophysical experiments demonstrated qualitatively similar performance to the ants and the computational and theoretical models. For example, measurement of the average flow rate,  $\bar{q}$ , of successful excavators (which we quantify here as the number of deposits per minute) revealed that excavation performance increased with an increasing number of robots in the trial ( $N$ ) until the system became sufficiently crowded (Fig. 4E).

To characterize how clustering led to performance degradation in the active protocol, we measured the frequency of cluster occurrences, denoted  $I_c$ . Here we defined clusters as groups of robots of number  $N_c$ , whose center positions were within a robot length of each other (supplementary materials). Such clusters occurred most frequently at the excavation site (histograms in Fig. 4, B to D), yielding phase separation (29) in the system, whereby a portion of robots were jammed at high density, whereas others moved smoothly through the tunnel at low density.

As in (9), we also measured the characteristic “relaxation” times for clusters using a tool from the study of glassy systems, the density overlap correlation function  $Q(\tau)$ .  $Q(\tau)$  compares the spatial overlap of a cluster at a specific time to the overlap of the cluster’s original lateral segment at a later time,  $\tau$ . Assuming a one-dimensional tunnel, we calculated the spatial overlap of robots by tracking their centroid position laterally (along the tunnel) and assigning intensity potentials in space, summing overlapping potentials of adjacent robots (fig. S12A). From these curves (Fig. 4G, inset; fig. S12; and supplementary materials), we calculated the relaxation time,  $\tau^*$ , for clusters of different  $N_c$  by fitting a stretched exponential function,  $Q_f(\tau) = \exp\left\{-\left(\frac{\tau}{\tau^*}\right)^\beta\right\}$ , to a  $Q$  curve averaged over clusters of the same  $N_c$ , where  $\beta$  is a fitting parameter that is of order unity.

The relaxation time analysis highlighted how sufficient numbers of active robots ( $N = 4$ ) resulted in clustering cascades. For example,  $N_c = 2$  robot clusters could be sufficiently difficult to resolve before a third robot joined the cluster, which in turn led to catastrophic  $N_c = 4$  robot jams that spanned the tunnel width. Such clogs were then difficult to resolve with the

robots’ limited sensory and motor capabilities and were likely exacerbated by the robots’ rigid oblong shape (Fig. 4F). A sharp increase in  $\tau^*$  for clusters with a linear density,  $\bar{\lambda}_c = N_c/L_c$ , where  $L_c$  is cluster length in body lengths, greater than unity (multirobot clusters) during four-robot active trials (Fig. 4H, green curve) revealed how this cascading scenario is reminiscent of glassy arrest in particulate systems (30, 31).

To discover how the strategies of idleness distributions and reversals affected clustering and traffic dynamics in the robots (movie S5), we implemented two protocols inspired by the biological observations and theoretical models. As in the CA model, in the Lorenz protocol (fig. S8), we implemented an unequal probability to enter the tunnel derived from experimental ant workload inequalities. We also implemented a separate robot reversal protocol (fig. S7), which produced selective retreats, whereby the robots were programmed to immediately resume excavation after deposition but reversed after not successfully reaching the excavation site within a given time. These strategies led to different excavation performances as  $N$  increased; but most importantly, both strategies outperformed the active protocol at  $N = 4$  (Fig. 4E).

The relaxation times and cluster analysis revealed the mechanisms by which the different protocols mitigated clogging, particularly in the distinct ways in which they reduced the duration of clusters and thus optimized the average occupancy of excavators, thereby improving traffic flow. For trials with up to three robots, all strategies produced a relatively low  $\tau^*$  (Fig. 4G) and frequency of cluster occurrence regardless of the number of robots in a cluster. However, for  $N = 4$ , the Lorenz and reversal protocols mitigated the clogging effects associated with the aggressive excavation in the active protocol.

The Lorenz and reversal protocols provided distinct forms of mitigating the catastrophic cascades of clogs found in the active protocol: Unequal workload distributions reduce the occurrence of clusters, and selective retreating limits the duration of clogs. Selective retreating in the reversal strategy limited the duration of clogs. Thus, instead of the glass-forming characteristics of active robots, clusters dissolved after some time, yielding low  $\tau^*$  (Fig. 4, G and H). The unequal workload distributions of the Lorenz strategy reduced the occurrence of clusters, especially the highest-density four-robot clusters (Fig. 4I), where glasslike clog formation is most likely to occur, resulting in fewer catastrophic clogs at the excavation site. We found similar evidence for clog mitigation in the analysis of clusters in the CA model (fig. S26 and supplementary materials), whereby clog mitigation was further found to be most effective when both strategies (reversals and unequal entrance probabilities) were used in combination.

To close, we return to the traffic aspects of the confined system: As in theory, traffic flow of robotic ants (which dominates the excavation performance) was maximal at an intermediate occupancy of excavators,  $\bar{\lambda} = N_T/W_T$ , where  $N_T$  is

the number of robots in the main tunnel area averaged across all frames of video and  $W_T$  is the width of the tunnel, followed by a gradual decline at higher  $\bar{\lambda}$  (fig. S11A). However, unlike the theoretical models, peak flow rate in robotic systems occurred at a  $\bar{\lambda}$  of approximately 0.25, which corresponds to less than one robot traversing the tunnel at a time, despite a tunnel width of about three robot widths, or 1.5 robot lengths.

We hypothesize that the underperformance of our robots relative to the biological and theoretical systems is a consequence of our robots’ limited mobility in confined spaces, indicating that deformable bodies (32) and novel locomotor mechanisms (12) will be important in confined real-world robot collectives. That said, given these strategies are robust to the vagaries of real-world interactions, we posit that other engineered systems—including robot swarms in disaster rubble, nanorobots surging through the bloodstream (33), and task-capable active materials (3)—could benefit from simple strategies that involve labor inequality, particularly in creative combinations (34).

## REFERENCES AND NOTES

1. A. Okubo, *Adv. Biophys.* **22**, 1–94 (1986).
2. M. Brambilla, E. Ferrante, M. Birattari, M. Dorigo, *Swarm Intell.* **7**, 1–41 (2013).
3. M. Marchetti et al., *Rev. Mod. Phys.* **85**, 1143–1189 (2013).
4. D. Helbing, *Rev. Mod. Phys.* **73**, 1067–1141 (2001).
5. N. C. Dantton, L. Turner, S. Rojevsky, H. C. Berg, *Biophys. J.* **98**, 2082–2090 (2010).
6. E. Méhes, T. Vicsek, *Integr. Biol. (Camb.)* **6**, 831–854 (2014).
7. A. Garcimartín et al., *Phys. Rev. E Stat. Nonlin. Soft Matter Phys.* **91**, 022808 (2015).
8. L. Giomi, N. Hawley-Weld, L. Mahadevan, *Proc. R. Soc. London A Math. Phys. Sci.* **469**, 20120637 (2013).
9. N. Gravish, G. Gold, A. Zangwill, M. A. D. Goodisman, D. I. Goldman, *Soft Matter* **11**, 6552–6561 (2015).
10. D. M. Gordon, *Nature* **380**, 121–124 (1996).
11. D. Cassill, W. R. Tschinkel, S. B. Vinson, *Insectes Soc.* **49**, 158–163 (2002).
12. N. Gravish, D. Monaenkova, M. A. Goodisman, D. I. Goldman, *Proc. Natl. Acad. Sci. U.S.A.* **110**, 9746–9751 (2013).
13. D. Monaenkova et al., *J. Exp. Biol.* **218**, 1295–1305 (2015).
14. V. Linevich, D. Monaenkova, D. I. Goldman, *Artif. Life Robot.* **21**, 460–465 (2016).
15. P. Tenczar, C. C. Lutz, V. D. Rao, N. Goldenfeld, G. E. Robinson, *Anim. Behav.* **95**, 41–48 (2014).
16. E. J. Robinson, O. Feinerman, N. R. Franks, *Proc. Biol. Sci.* **276**, 4373–4380 (2009).
17. D. M. Gordon, *Cell Syst.* **3**, 514–520 (2016).
18. V. Fourcassié, A. Dussutour, J. L. Deneubourg, *J. Exp. Biol.* **213**, 2357–2363 (2010).
19. A. John, A. Schadschneider, D. Chowdhury, K. Nishinari, *J. Theor. Biol.* **231**, 279–285 (2004).
20. N. Gravish et al., *J. R. Soc. Interface* **9**, 3312–3322 (2012).
21. C. R. Reid et al., *Proc. Natl. Acad. Sci. U.S.A.* **112**, 15113–15118 (2015).
22. C. Gershenson, D. Helbing, *Complexity* **21**, 9–15 (2015).
23. K. Nagel, M. Schreckenberg, *J. Phys.* **12**, 2221–2229 (1992).
24. R. Kühne, in *Highway Capacity and Level of Service: Proceedings of the International Symposium on Highway Capacity, Karlsruhe, 24–27 July 1991*, U. Brannolte, Ed. (CRC Press, 1991).
25. H.-S. Kuan, M. D. Betterton, *Phys. Rev. E* **94**, 022419 (2016).
26. J. Aguilar et al., *Rep. Prog. Phys.* **79**, 110001 (2016).
27. M. J. Mataric et al., in *From Animals to Animals 2: Proceedings of the Second International Conference on Simulation of Adaptive Behavior*, J.-A. Meyer, H. L. Roitblat, S. W. Wilson, Eds. (MIT Press, 1993), pp. 432–441.
28. U. Borrmann, L. Wang, A. D. Ames, M. Egerstedt, *IFAC-PapersOnLine* **48**, 68–73 (2015).
29. G. S. Redner, M. F. Hagan, A. Baskaran, *Phys. Rev. Lett.* **110**, 055701 (2013).

30. D. I. Goldman, H. L. Swinney, *Phys. Rev. Lett.* **96**, 145702 (2006).
31. H.-S. Kuan, R. Blackwell, L. E. Hough, M. A. Glaser, M. D. Betterton, *Phys. Rev. E Stat. Nonlin. Soft Matter Phys.* **92**, 060501 (2015).
32. K. Jayaram, R. J. Full, *Proc. Natl. Acad. Sci. U.S.A.* **113**, E950–E957 (2016).
33. S. Li *et al.*, *Nat. Biotechnol.* **36**, 258–264 (2018).
34. W. Liu, A. F. Winfield, J. Sa, J. Chen, L. Dou, *Adapt. Behav.* **15**, 289–305 (2007).

#### ACKNOWLEDGMENTS

The authors thank W. Gardner, Griffin Botanical Garden, and Chattahoochee-Oconee National Forest for giving us permission for ant collection. We would also like to acknowledge N. Gravish for insight and fruitful discussions; M. Kingsbury and L. Chen for

assistance in magnetic particle construction; R. Kutner, R. Srivastava, and J. Logan for their help with video analysis; and N. Conn for help with ant collection. H.-S.K. thanks the Max Planck Institute for the Physics of Complex Systems for providing computing resources. **Funding:** The authors acknowledge the support of National Science Foundation grants NSF PoLS-0957659, PHY-1205878, and DMR-1551095, as well as ARO grant W911NF-13-1-0347, the National Academies Keck Futures Initiative, and the Dunn Family Professorship (to D.I.G.). **Author contributions:** B.D. and D.M. collected the raw data for the ant experiments. W.S. and D.M. developed and performed the CA simulations. H.-S.K. and M.D.B. developed and analyzed the OAT model. V.L. constructed and performed the ant robot experiments, and J.A. tracked and analyzed the robot experiment data. All authors contributed to the preparation of the manuscript and were involved in the interpretation of results. **Competing interests:** The

authors declare that they have no competing interests. **Data and materials availability:** Data are available on SMARTech at <https://smartech.gatech.edu/>.

#### SUPPLEMENTARY MATERIALS

[www.sciencemag.org/content/361/6403/672/suppl/DC1](http://www.sciencemag.org/content/361/6403/672/suppl/DC1)  
Materials and Methods  
Figs. S1 to S26  
Tables S1 to S4  
References (35–41)  
Movies S1 to S5

6 April 2017; resubmitted 17 January 2018  
Accepted 14 June 2018  
10.1126/science.aan3891

## Collective clog control: Optimizing traffic flow in confined biological and robophysical excavation

J. Aguilar, D. Monaenkova, V. Linevich, W. Savoie, B. Dutta, H.-S. Kuan, M. D. Betterton, M. A. D. Goodisman and D. I. Goldman

*Science* **361** (6403), 672-677.  
DOI: 10.1126/science.aan3891

### When fewer workers are more efficient

A narrow passageway can easily become clogged or jammed if too much traffic tries to enter at once or there is competition between the flow of traffic in each direction. Aguilar *et al.* studied the collective excavation observed when ants build their nests. Because of the unequal workload distribution, the optimal excavation rate is achieved when a part of the ant collective is inactive. Numerical simulations and the behavior of robotic ants mimic the behavior of the colony.

*Science*, this issue p. 672

#### ARTICLE TOOLS

<http://science.sciencemag.org/content/361/6403/672>

#### SUPPLEMENTARY MATERIALS

<http://science.sciencemag.org/content/suppl/2018/08/15/361.6403.672.DC1>

#### REFERENCES

This article cites 36 articles, 8 of which you can access for free  
<http://science.sciencemag.org/content/361/6403/672#BIBL>

#### PERMISSIONS

<http://www.sciencemag.org/help/reprints-and-permissions>

Use of this article is subject to the [Terms of Service](#)